International Journal of Minerals, Metallurgy and Materials
Volume 26, Number 5, May 2019, Page 611
https://doi.org/10.1007/s12613-019-1769-x

Effect of electroslag remelting and homogenization on hydrogen flaking in AMS-4340 ultra-high-strength steels

Shivraj Singh Kasana[1,2] *and O.P. Pandey*[1]

1) School of Physics and Materials Science, Thapar Institute of Engineering and Technology, Patiala 147004, India
2) Star Wire (India) Ltd. Ballabgarh, Haryana 121004, India
(Received: 28 June 2018; revised: 9 December 2018; accepted: 13 December 2018)

Abstract: Hydrogen flakes and elemental segregation are the main causes of steel rejection. To eliminate hydrogen flaking, the present study focuses on the manufacture of AMS-4340 ultra-high-strength steel through an alternate route. AMS-4340 was prepared using three different processing routes. The primary processing route consisted of melting in an electric arc furnace, refining in a ladle refining furnace, and vacuum degassing. After primary processing, the heat processes (D1, D2, and D3) were cast into cylindrical electrodes. For secondary processing, electroslag remelting (ESR) was carried out on the primary heats to obtain four secondary heats: E1, E2, E3, and E4. Homogenization of ingots E1, E2, E3, and E4 was carried out at 1220°C for 14, 12, 12, and 30 h, respectively, followed by an antiflaking treatment at 680°C and air cooling. In addition, the semi-finished ESR ingot E4 was again homogenized at 1220°C for 6–8 h and a second antiflaking treatment was performed at 680°C for 130 h followed by air cooling. The chemical segregation of each heat was monitored through a spectroscopy technique. The least segregation was observed for heat E4. Macrostructure examination revealed the presence of hydrogen flakes in heats E1, E2, and E3, whereas no hydrogen flakes were observed in heat E4. Ultrasonic testing revealed no internal defects in heat E4, whereas internal defects were observed in the other heats. A grain size investigation revealed a finer grain size for E4 compared with those for the other heats. Steel produced in heat E4 also exhibited superior mechanical properties. Therefore, the processing route used for heat E4 can be used to manufacture an AMS-4340 ultra-high-strength steel with superior properties compared with those of AMS-4340 prepared by the other investigated routes.

Keywords: AMS-4340 steel; segregation and homogenization; antiflaking treatment; electroslag remelting

1. Introduction

Steels are widely used engineering materials. Different types of steels are used in various applications in the automotive, aerospace, and defense sectors. The mechanical properties of steels are highly influenced by the processing routes used to manufacture them. Sharma *et al*. [1] analyzed the importance of processing parameters on the mechanical properties of steels and concluded that, with modification of the processing parameters, superior mechanical properties can be achieved even for very low-carbon steels.

Despite numerous improvements in steelmaking processes (e.g., electric arc furnace (EF) melting, refining, and vacuum degassing (VD)), ultrasonic defects and chemical segregation account for the majority of steel quality-control failures. Pickering [2] observed that components are rejected and scrapped mostly because of defects such as segregation. The ultra-high-strength steels (UHSSs) alloyed with Ni, Cr, Mo, and V are more prone to hydrogen flaking than other UHSSs. Liu *et al*. [3] have observed that segregation of Ni, Cr, and C occurs from the bottom to the top and also from the surface to the center of UHSSs during electroslag remelting (ESR) because of gravitational and thermal buoyancy effects.

Prasad and Wanhill [4] have observed that hydrogen flaking is a major reason for the quality-control failure of UHSSs, especially those developed for defense applications. Various UHSSs such as AISI 4130, 4140, and 4340 are used in defense applications such as gun barrels and ballistic projectiles. Majumdar and Sadhukhan [5] manufactured

Corresponding author: O.P. Pandey E-mail: oppandey@thapar.edu

Ni–Cr–Mo–V UHSS for gun-barrel applications using an alternative route and observed an improvement in mechanical properties. UHSSs should be ultra-clean steels with little elemental segregation to ensure that their mechanical properties are isotropic. For this application, the manufacturing of UHSSs is carried out under vacuum via the vacuum induction melting (VIM) process followed by vacuum arc remelting (VAR). Choudhury [6] reported that, for very low concentrations of hydrogen and exceptionally clean steels, VIM is necessary and that VAR and ESR can also be used if the environmental factors are properly controlled. The steels processed by VD and remelting exhibit numerous advantages, e.g., reduced nonmetallic inclusions, reduced gas levels, and superior cast structures, over steels prepared by air melting. However, the process itself is very expensive and the overall cost of the finished material is very high. Steneholom *et al*. [7] observed that VD is important for manufacturing clean steel; i.e., the steel should be free from oxygen, sulfur, and other impurities.

Several authors have investigated the manufacture of UHSSs using ESR and have found that the majority of the produced UHSSs failed inspection because of hydrogen flaking. Ali *et al*. [8] observed that the ESR process is one of the most important secondary refining processes because of its relatively low production cost, low capital investment, and ability to produce high-quality steels. Furthermore, to manufacture UHSSs, not only the chemical composition of the slag but also the activity of the elements in the molten metal should be taken into account. Johnson [9] observed that the hydrogen in steels diffuses at the atomic level, which leads to an increase in hydrogen embrittlement of the steels. Ćwiek [10] suggested different methods of mitigating hydrogen degradation, including degradation by hydrogen embrittlement, hydrogen-induced blistering, cracking due to precipitation of internal hydrogen (hydrogen flaking), hydrogen attack, and cracking due to hydride formation. Fruehan [11] suggested an antiflaking treatment (AFT) path to induce the austenite-to-bainite transformation while minimizing hydrogen flaking and elemental segregation and avoiding the austenite-to-martensite transformation during post-forging. Vrbek *et al*. [12] described the changes in the solubility of hydrogen at various stages of the steel manufacturing process and also suggested different methods to measure hydrogen content in the liquid and solid states. Voronenko [13] reviewed the different reasons for hydrogen flaking and inclusions in steels. AFTs as a remedy have also been described. Konopel'ko *et al*. [14] developed a method to measure the concentration of hydrogen in steels. They observed that vacuum techniques for measuring the concentration of hydrogen can provide reliable results compared with the method of heating and melting in a carrier gas. Dimitriu and Popescu [15] observed that the hydrogen flakes in steels can be removed during hot plastic deformation.

UHSSs such as AMS-4340 are normally manufactured through VIM followed by VAR. However, this process is quite expensive. The aim of the present work is to develop a low-cost alternative for manufacturing AMS-4340 UHSS. Furthermore, characterization (macrostructure and microstructure) and testing (ultrasonic testing, mechanical testing) has also been carried out to evaluate the quality of the produced steel.

2. Experimental

2.1. Materials

In the present investigation, AMS-4340 was manufactured for defense applications, especially for use in gun barrels. Table 1 presents the designated and permissible chemical composition for AMS-4340 steel.

Table 1. Permissible and designated steel chemistry for AMS-4340 grade steel wt%

Element	C	Si	Mn	P	S	Cr	Mo	Ni	Cu	Al	V
Permissible limit	0.38–0.43	0.15–0.35	0.65–0.90	0.010 (Max.)	0.010 (Max.)	0.70–0.90	0.20–0.30	1.65–2.00	0.35 (Max.)	—	—
Designed limit	0.40	0.25	0.86	0.007	Lowest	0.86	0.27	1.89	Lowest	0.02	0.05–0.10

2.2. Processing route

Fig. 1 presents a detailed flow chart of the processes used to manufacture AMS-4340 UHSS. The entire process is designed to achieve a standard chemistry and required properties for AMS-4340 steel. The steel is melted in an EF followed by refining in a ladle refining furnace (LF) and VD.

The steel was cast into cylindrical electrodes, which were further subjected to ESR under an inert argon atmosphere. After ESR, the steel was annealed, hot-press forged, and normalized. Samples were prepared for quality and testing evaluation. Three different heat processes (D1, D2, and D3) were prepared using the processing route shown in Fig. 1. D1, D2, and D3 represent the primary processing steps including EF, LF, VD, and casting into cylindrical electrodes. Table 2 presents the detailed processing parameters for

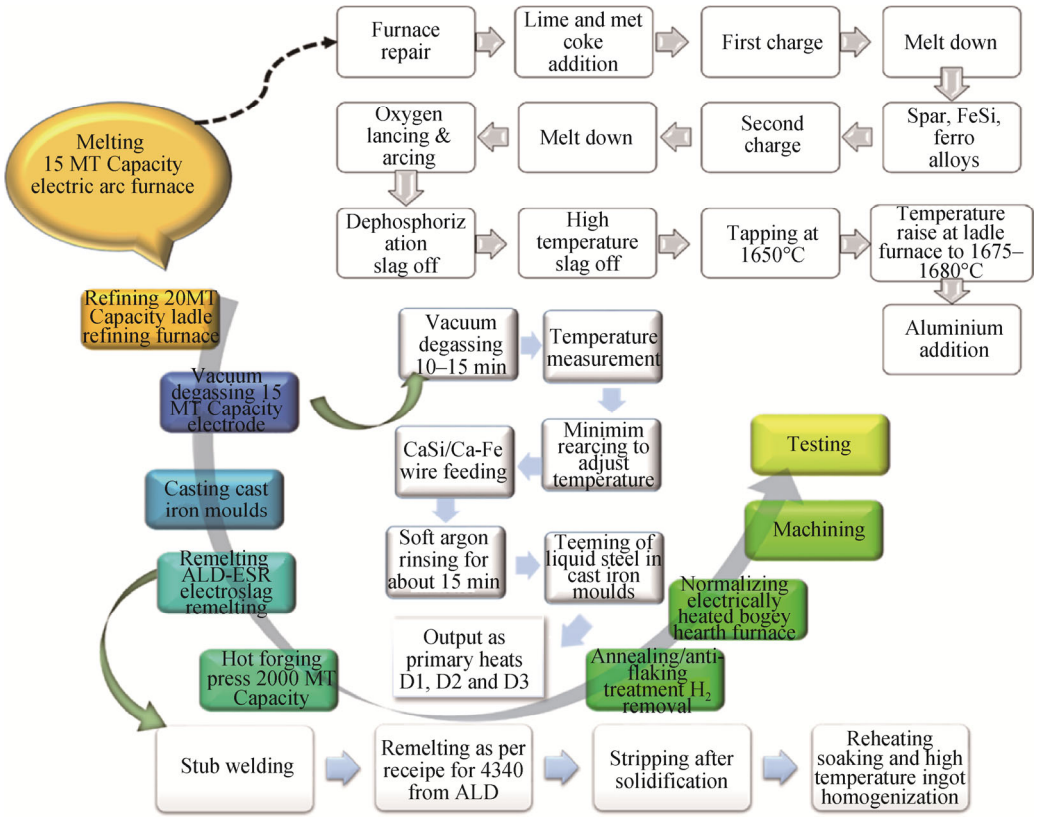

Fig. 1. Process for manufacturing AMS-4340 UHSS.

Table 2. Melting, refining and casting parameters for primary heats

Process parameter	Heat No.		
	D1	D2	D3
Charge weight / kg	14520	13170	14510
Charge mix	Mild steel scrap 8870 kg + DMR249 steel scrap 2150 kg + alloy steel with 3wt% Ni 3500 kg + lime 180 kg. Total metallic charge is 14520 kg	Mild Steel scrap 8270 kg + DB6 tool steel scrap 2100 kg + alloy steel with 3wt% Ni 2350 + skull 4340 450 kg + lime 180 kg + M/coke 300 kg. Total metallic charge is 13170 kg	Mild Steel scrap 4750 kg + 21Cr steel scrap 2020 kg + alloy steel with 3wt% Ni 7230 kg + alloy steel with 3% Ni Mo(0.40wt%) 510 kg + lime 200 kg + M/coke 300 kg. Total metallic charge is 14510 kg
Tapping temperature / °C	1643	1642	1655
Mould temperature / °C	72	76	82
Temperature before vacuum degassing / °C	1675	1635	1645
H_2 before vacuum degassing / ppm	5.1	4.7	3.7
Vacuum degassing hold time at low pressure / min	10	12	15
Vacuum pressure level / (10^2 Pa)	1	0.9	0.7
H_2 after vacuum degassing / ppm	1.7	1.7	1
Temperature after Vacuum degassing / °C	1517	1552	1538
Re-arcing time to achieve the ladle / min	30	15	10
CaSi wire feeding (0.034 kg·m^{-1}) / m	0	0	60
Al level before Ca feeding / wt%	0.03	0.04	0.04
Teeming time / min	28.10	17.05	20.50
Feeding time / min	5.30	4.27	4.20
Ar flow in shroud / (L·min^{-1})	72	68	64
Cylindrical electrode	DIA. 720-01PCS	DIA.-480-02PCS	DIA. 720-01PCS
Cast weight / kg	13400	12200	13500

manufacturing primary heats D1, D2, and D3. Further, the primary heats were subjected to ESR. The primary heat D1 was converted to ESR heat E1, D2 was converted to ESR heats E2 and E3, and D3 was converted to ESR heat E4. Primary heats D1and D3 each consisted of one cylindrical electrode of diameter 720 mm. By contrast, primary heat D2 consisted of two cylindrical electrodes of 480-mm diameter. Thus, after ESR, primary heat D2 was converted to two ESR heats (E2 and E3). Fig. 2 and Table 3 present the various ESR processing parameters for ESR heats E1, E2, E3, and E4. Further, the inert gas intake flow for the ESR process was kept constant at 10 L/min.

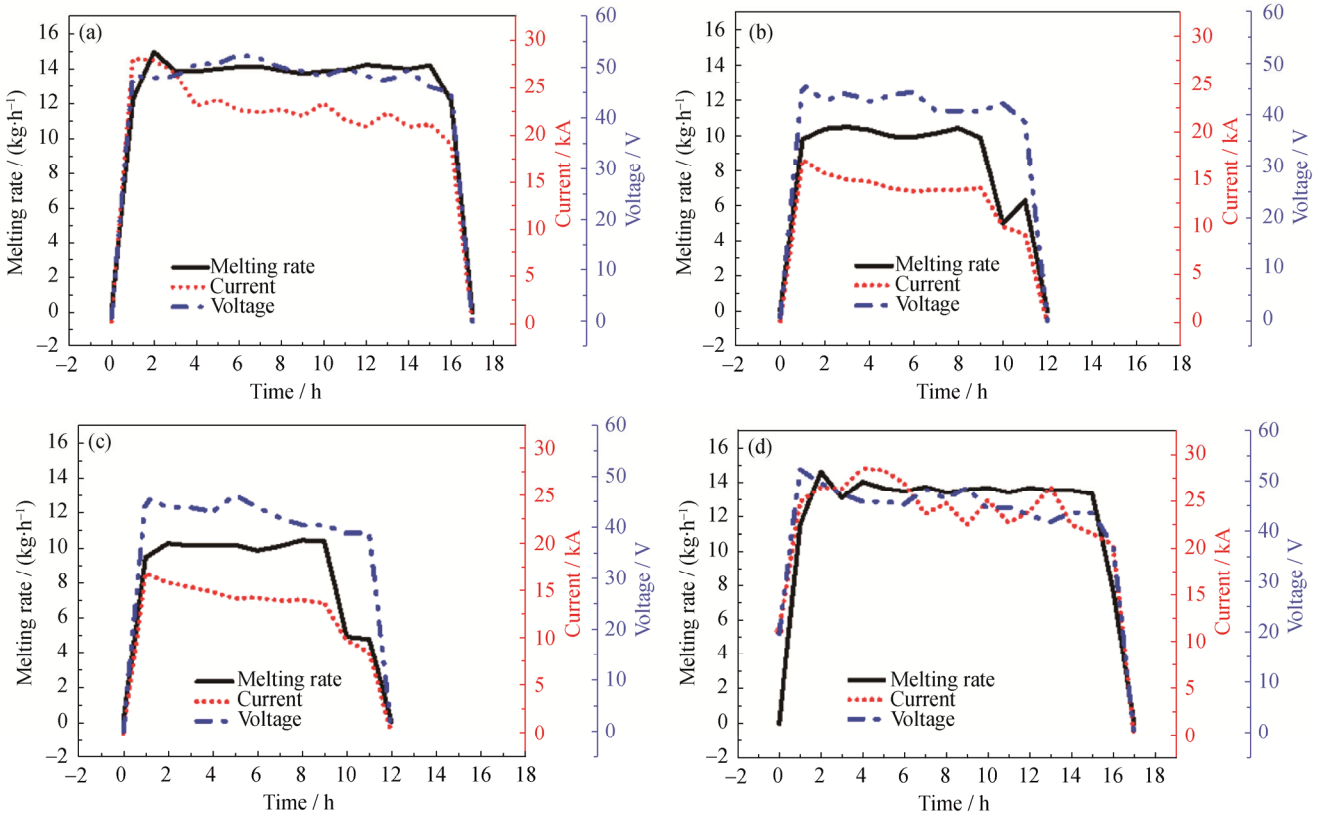

Fig. 2. Voltage, current, and melting rate parameters for ESR heats E1 (a), E2 (b), E3 (c), and E4 (d).

Table 3. ESR process parameters

Primary heat No.	ESR heat No.	Diameter / mm	Melt rate / (kg·min^{-1})					
			Start phase		Melt phase		Hot topping	
			Min.	Max.	Min.	Max	Min.	Max.
D1	E1	900	0	15.49	13.5	14.95	8.61	14.31
D2	E2	600	0	10.54	9.69	10.68	4.55	10.23
	E3			10.11	9.7	11.23	4.02	10.16
D3	E4	900	0	16.47	12.7	14.25	4.37	13.56

Table 4 presents the slag consumption for different ESR heats E1, E2, E3, and E4. Slag helps in capturing the non-metallic inclusions during the ESR process. In the present work, Wacker 2037 ELH slag, which is an extra-low-hydrogen slag, was used. Table 5 presents the chemical composition of the Wacker 2037 ELH slag. This slag was used as per the recommendation of the ESR furnace supplier. A new sealed drum of 2037 ELH slag was opened in every melting. The unused leftover slag in the drum was further protected from the atmosphere by being stored under a positive pressure of dry, ultra-high-purity argon.

Table 4. Slag consumption in respective ESR heats kg

ESR heat No.	Total	Initial	Using slag feeder	Used slag
E1	250	30	220	125
E2 and E3	110	20	90	55
E4	250	30	220	Not used

Table 5. Chemical composition of Wacker 2037 ELH slag wt%

CaF_2	CaO	Al_2O_3
60	20	20

After remelting, ESR ingots E1, E2, and E3 were subjected to heating, soaking/homogenization and forging, followed by an AFT. For ESR ingot E4, two AFTs were applied: one in semistage and the other after finish forging.

After the AFT, the samples were air cooled to room temperature. Fig. 3 presents the time–temperature curves for heating soaking and high-temperature homogenization and forging cycles for ESR ingots E1, E2, E3, and E4. For ESR ingot E1, homogenization was carried out at 1220°C for 14 h; for ESR ingots E2 and E3, homogenization was carried out at 1220°C for 12 h.

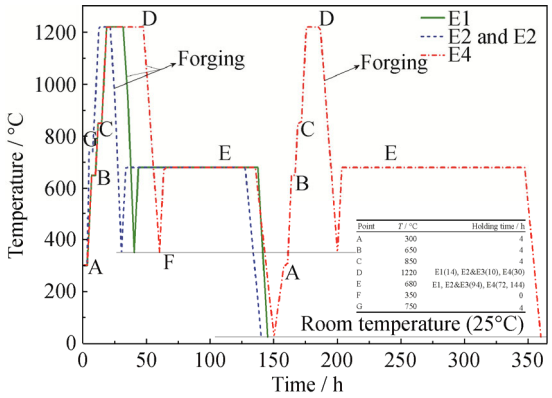

Fig. 3. Heating soaking and high-temperature homogenization and forging cycles for ESR ingots E1, E2, E3, and E4.

For the ESR ingot, E4 homogenization was carried out at 1220°C for 30 h before hot forging. The ESR ingots E1, E2, and E3 were hot forged from initial diameters of 900 mm, 600 mm, and 600 mm, respectively, to a diameter of 340 mm. ESR ingot E4 was semi-forged from a diameter of 900 mm to a diameter of 500 mm. After forging, ESR ingots E1, E2, E3, and E4 were subjected to an AFT at 680°C followed by air cooling. The semi-finished ESR ingot E4 was again heated and homogenized at 1220°C for 6–8 h, finish forged (from a diameter of 500 mm to a diameter of 340 mm), and subsequently subjected to second AFT at 680°C for 130 h, followed by air cooling [16–19]. ESR Heat E1 was forged from a 900-mm-diameter ingot by drawing and then upsetting to a diameter of 340 mm, resulting in an overall reduction ratio greater than 10.5:1. ESR heats E2 and E3 were forged from 600-mm diameter by drawing–upsetting–drawing–upsetting–drawing to 340-mm diameter to achieve overall reduction greater than 10.6:1. Similarly, ESR heat E4 was forged from a 900-mm diameter by drawing–upsetting–drawing–upsetting–drawing to achieve an overall reduction ratio greater than 11.8:1. The forged bars were normalized, tempered, and machined to the desired specifications. For macrostructure investigations and to distinguish the hydrogen flakes, a transverse slice of 320-mm diameter and 30-mm thickness was cut. A 50-mm-wide slice was cut from this circular sample and polished with 120-, 240-, 400-, and 600-grit polishing paper, followed by 20–25 min of hot-acid etching by being boiled in commercial hydrochloric acid to reveal the hydrogen flakes, as per standard ASTM A604. Macrographs of part of a 50 mm × 80 mm area were recorded. To observe various structural features of the ESR heats, microstructural characterization was carried out using an optical microscope (Zeiss-Axio Observer D1M, Carl Zeiss, Germany). Mechanical properties were further evaluated on a universal testing machine (DX-600, Instron, USA) according to standard ASTM A370. Impact testing (IT-30, FIE, India) was performed at sub-zero temperature (−40°C) according to standard ASTM A370. Segregation of different alloying elements was observed through a spectroscopy technique (Spectro Lab M9, Germany). For segregation analysis, a transverse slice of steel of 340 mm in diameter and 25 mm thick was cut. From this slice, a transverse rectangular slice of 175 mm × 30 mm was cut from the central part.

3. Results and discussion

3.1. Chemical composition

Table 6 presents the chemical composition of the primary heats D1, D2, and D3. Table 7 presents the chemical composition of ESR heats E1, E2, E3, and E4 after finish forging and normalizing. ESR was performed under an inert argon atmosphere, which led to a decrease in the levels of macro- and microsegregation. Advancements in ESR furnace technology enable accurate control of the operating parameters. The process parameters of the ingots manufactured

Table 6. Chemical composition and of the primary heats wt%

Primary heat No.	C	Si	Mn	P	S	Cr	Mo	Ni	V	W	N	H
D1	0.395	0.255	0.86	0.007	0.002	0.88	0.26	1.87	0.005	0.001	0.007	0.00017
D2	0.400	0.26	0.85	0.008	0.002	0.84	0.28	1.865	0.01	0.02	0.005	0.00018
D3	0.395	0.25	0.775	0.008	0.001	0.83	0.275	1.92	0.004	0.008	0.0026	0.0001

Table 7. Chemical composition of the ESR heats after finish forging and normalizing wt%

ESR heat No.	C	Si	Mn	P	S	Cr	Mo	Ni	V	W	N	H
E1	0.410	0.250	0.84	0.007	0.002	0.85	0.252	1.83	0.06	0.001	0.0078	0.00019
E3	0.410	0.25	0.87	0.007	0.002	0.82	0.27	1.825	0.07	0.018	0.0057	0.0002
E3	0.410	0.25	0.87	0.007	0.002	0.82	0.27	1.823	0.07	0.02	0.0057	0.0002
E4	0.415	0.248	0.83	0.007	0.001	0.80	0.263	1.82	0.08	0.004	0.0031	0.00013

via the ESR route were critically and accurately controlled, which was expected to lead to the development of a very sound solidified structure with good homogeneity and without any internal defects [20–22].

Because of the good chemical homogeneity in the ingot, high-temperature homogenization prior to the hot forging process (thermomechanical treatment) results in isotropy in the forgings after ESR. The mechanical properties achieved after thermomechanical processing and heat treatment result in similar mechanical properties in both the longitudinal and transverse directions upon forging after ESR [20,23].

Fig. 3 presents the variation in composition of the major alloying elements along the diameter, starting from the surface. As observed in Fig. 4, ESR heat E4 shows minimum segregation compared with heats E1, E2, and E3. This less extensive segregation is attributed to the additional high-temperature homogenization and two-stage AFT of heat E4.

Although two homogenization and antiflaking cycles were highly effective for preventing microscopic segregation, unsatisfactory spectroanalysis results were obtained for ESR heats E1, E2, and E3. To improve the macroelemental segregation, ESR heat E4 was subjected to a longer homogenization treatment than ESR heats E1, E2, and E3. ESR heat E4 (with the longest homogenization cycle and two AFTs) showed the least elemental segregation and maximum diffusion of hydrogen on the macroscale.

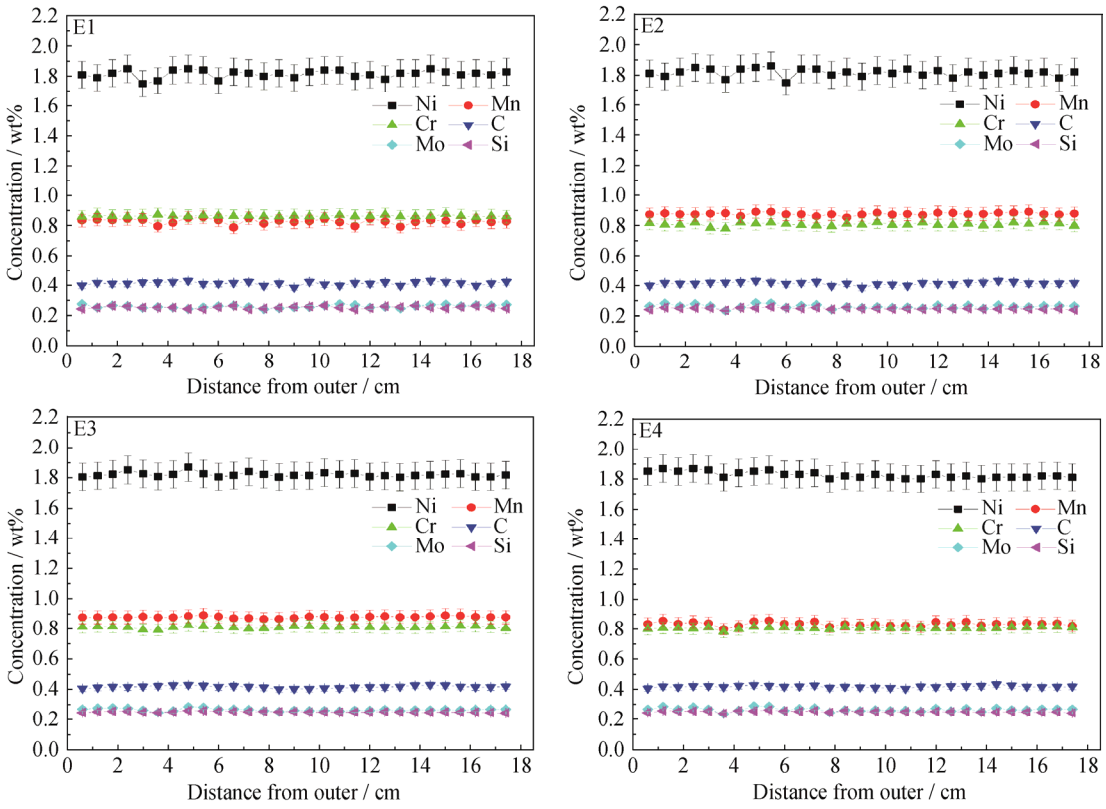

Fig. 4. Segregation of the alloying elements in E1, E2, E3, and E4.

3.2. Macrostructural examination

Table 8 presents different macroscopic features observed in the samples. Fig. 5(a) presents the macrostructure of hydrogen flakes, as observed on a 50 mm × 80 mm sample of one of the ESR heats, E1. Similar hydrogen flakes were also observed in ESR heats E2 and E3. However, ESR heat E4 was free from hydrogen flakes (Fig. 5(b)).

Table 8. Macrostructure examination of ESR heats

ESR heat No.	Flute crack	Sponginess	Flakes	Dendrites
E1	Absent	Absent	Present	Present
E2	Absent	Absent	Present	Present
E3	Absent	Absent	Present	Present
E4	Absent	Absent	Absent	Present

The dissolved hydrogen in the steels tends to be absorbed at sites such as segregation regions and nonmetallic inclusions [11]. For E1, E2, and E3, the soaking and homogenization at 1220°C for nearly 20–30 min/inch was likely insufficient to minimize segregation, possibly leading to the development of sites for hydrogen accumulation. Thus, an increase in the threshold of hydrogen was observed. This critical amount of hydrogen manifests as flaking [11]. By contrast, for E4, an additional homogenization of approximately 20 min/inch led to the distribution of segregation, which in turn led to a decrease in the accumulation of hydrogen below the hydrogen flaking threshold value. In addition, a reduction in hydrogen flaking was observed with the two-stage AFT performed on E4 (i.e., one treatment with E4 in the semi-forged stage and the other after final forging).

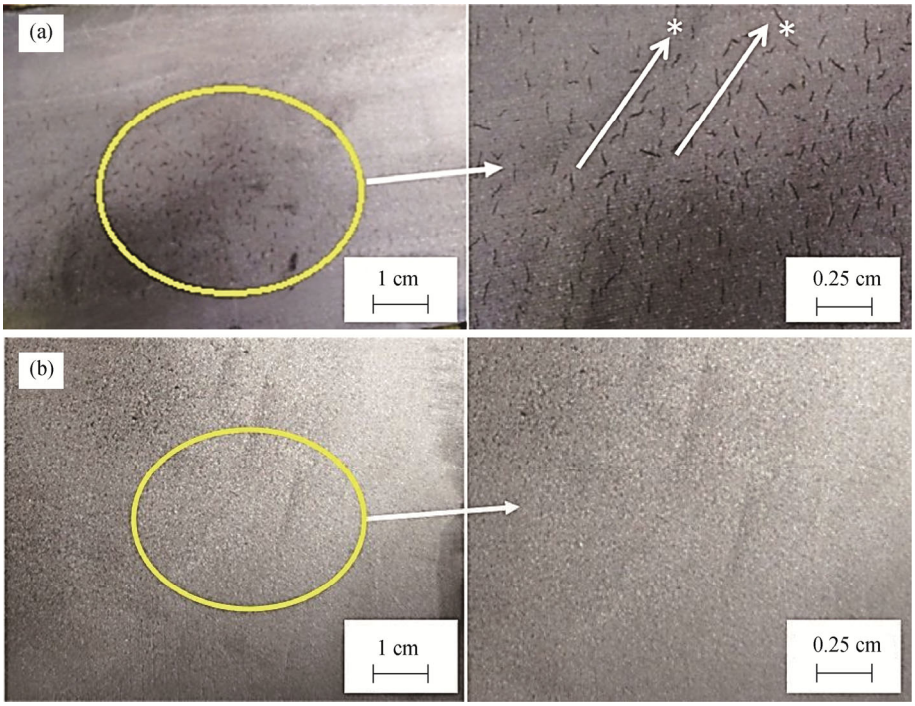

Fig. 5. Macrostructure examination of ESR heats E1 (a) and E4 (b). Symbol "*" indicates aligned hydrogen inclusions leading to crack initiation.

3.3. Microstructure analysis

Fig. 6 presents the microstructural features of ESR heats normalized at 870°C and tempered at 675°C. Fig. 6(a) presents the structure of the E1 steel. The structure is a coarse tempered martensitic/bainitic type. Some fine carbides are also present. Consequently, the yield point was reduced. Fig. 6(b) presents the microstructure of the E2 steel, whose structure is similar to that of the ESR heat E1 steel. However, some randomly oriented carbides are also seen. These carbides may enhance the yield point and the ultimate tensile strength. As shown in Fig. 6(c), the features observed in the E1 and E2 steels are absent in the E3 steel. The structure corresponding to the E3 steel shows a homogenous distribution of all present phases. This structure is more refined, which may lead to better ductility and higher strength. The colonial growth of phases observed in steels E1 and E2 is absent. The structure may exhibit isotropic properties. However, some growth of the tempered microstructure is observed. The microstructure observed for the E4 steel is more refined. The phases are uniformly distributed and, most importantly, the aligned growth of different phases is absent. When compared with the E1 and E2 steels, the E4 steel exhibits more refined features. Although the phases observed for the E4 steel are similar to those of the E3 steel, the E4 steel exhibits a more refined structure, possibly because of the additional homogenization and AFT applied to ESR heat E4. The structural properties of these steels are consistent with their mechanical properties.

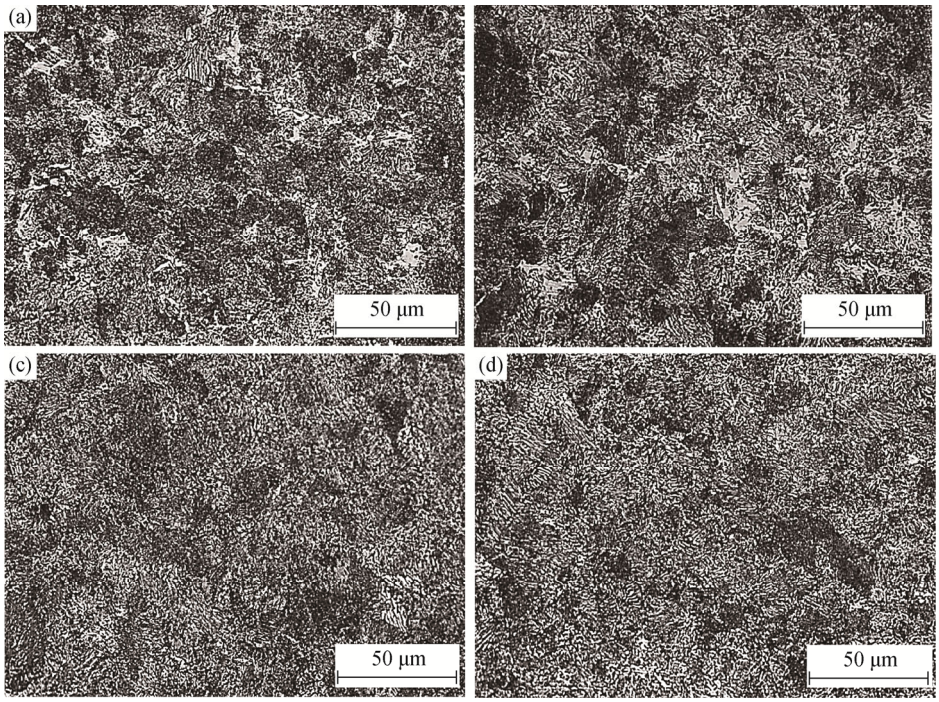

Fig. 6. Microstructural characterization of ESR heats normalized at 870°C and tempered at 675°C for steels: (a) E1; (b) E2; (c) E3; (d) E4.

Fig. 7 presents the structural features of ESR heats E1, E2, E3, and E4 after hardening (870°C) and tempering (240°C) treatments. The structural features here are also consistent with those observed in Fig. 6. A higher hardening temperature led to a coarser structure for steel E1. In addition, the strain induced in the steel may have been relaxed during hardening treatment, leading to the development of some colonial patches, as evident in Fig. 7(a). Such structural features indicate some type of segregation of the alloying elements, which were redistributed during the hardening and tempering treatment. Hydrogen may become trapped at these sites. Fig. 7(b) presents the microstructure of the E2 steel. The structure is more refined and homogenized compared with that of the E1 steel. However, a coarser structure is observed in some areas compared with other areas. A mixed structure comprising martensite and bainite is observed. Fig. 7(c) presents the structure of the E3 steel. The microstructural features of the E2 and E3 steels are similar. The only difference observed is the lack of colonial growth in the E3 steel. However, in certain locations, the carbide phase is aligned. Fig. 7(d) presents the microstructure of the E4 steel. Compared with the microstructure of the E1, E2, and E3 steels, that of the E4 steel is more refined and uniform. The growth of all of the phases present in the E4 steel is uniform and isotropic in nature.

While analyzing the structural features in Figs. 6 and 7, we observed that the heat treatment cycles applied to the E4 steel led to the development of a refined and uniform structure. Such structures led to the distribution of hydrogen flakes throughout the structure. Such distribution of hydrogen flakes may not lead to a stress concentration zone, thereby avoiding failure of the steel. Fig. 8 depicts the microstructural features of a crack that originated from hydrogen flakes in ESR heat E1. As shown in Fig. 5(a) (marked by an arrow) the cracks originate from the hydrogen flakes, join together, and propagate further in due course. The variation in crack thickness from one point to another point is a clear indication that cracks originate from these flakes and further move to other cracks, as shown in Fig. 8. The origin of such growth can also be seen in other areas of the structure. Such features may lead to a decrease in strength and ductility of the material. They may also lead to the catastrophic failure of steels.

3.4. Testing and evaluation

Ultrasonic testing was performed to observe the internal defects of the ESR heats. Because of the presence of hydrogen flakes in heats E1, E2, and E3, the rate of rejection for ultrasonic defects is very high. For ESR heats E1 and E4, a maximum rejection of 80% and no rejection are observed, respectively. Table 9 presents the ultrasonic test results obtained as per Rafael Specification No. 5036 R4 and AMS 2370 with a 1.2-mm flat-bottomed hole reference; a USN-60 (Kraut Kramer) flaw detector was used in conjunction with a B-4S-(57746) probe with a 24-mm diameter and a horizontal range 0–350 mm covering 360°, where Mobil oil was used as the couplant.

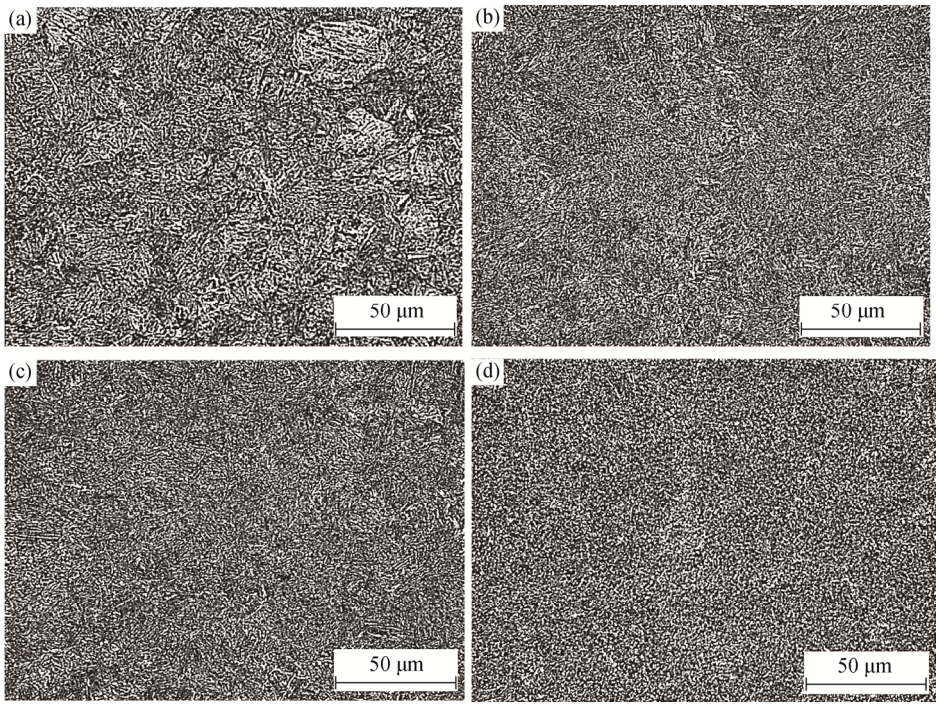

Fig. 7. Microstructure of ESR heats after a final heat treatment process consisting of hardening at 870°C and tempering at 240°C for steels: (a) E1; (b) E2; (c) E3; (d) E4.

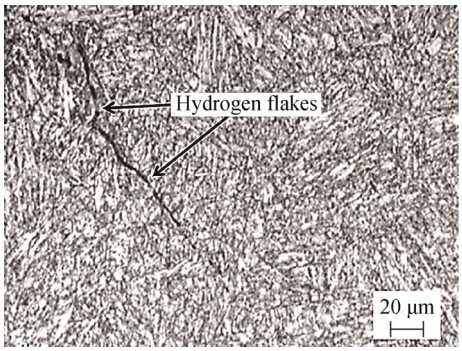

Fig. 8. Microstructural features of the hydrogen flakes of ESR heat E1.

Table 9. Ultrasonic testing results for different ESR heats

ESR heat No.	Total forged length / mm	Workable length / mm	Rejected length / mm	Rejection / %
E1	14500	2200	11800	~80
E2	6500	1950	4550	~70
E3	6500	2070	4430	~68
E4	14300	14300	0	0

Table 10 shows the nonmetallic inclusions present in different ESR heats. Because the same ESR process was used in the manufacturing of E1, E2, E3, and E4, negligible variations in the nonmetallic inclusions were observed. A finer grain size was observed for ESR heat E4 in comparison with those for ESR heats E1, E2, and E3 (Table 11). The refinement of the grain size led to the improvement in the mechanical properties of ESR heat E4. Table 12 presents the target mechanical properties and the mechanical properties achieved for ESR heats E1, E2, E3, and E4. ESR heat E1 was rejected because it did not achieve the desired yield strength. ESR heats E2 and E3 exhibited the desired mechanical properties but were rejected during the ultrasonic testing. ESR heats E2 and E3 achieved the desired mechanical properties because of their smaller-diameter ingots. ESR heat E4 achieved the best combination of mechanical properties because of the longer high-temperature homogenization and two-stage AFT. The processing route used for ESR heat E4 resulted in the best properties (ultrasonic and mechanical), and this material was accepted.

Table 10. Non-metallic inclusions (As per ASTM E45 Method A)

ESR heat No.	Type A		Type B		Type C		Type D	
	Thin	Thick	Thin	Thick	Thin	Thick	Thin	Thick
E1	0	0	1.5	0.5	0	0	1.0	0.5
E2	0	0	1.0	0.5	0	0	1.0	0.5
E3	0	0	1.0	0.5	0	0	1.0	0.5
E4	0	0	0.5	0.5	0	0	0.5	0

Table 11. Grain size of different ESR heats (As per ASTM E-112 standard)

ESR heat No.	Grain size (ASTM)
E1	5.0
E2	5.0–5.5
E3	5.0–5.5
E4	6.5–7.0

Table 12. Desired and achieved mechanical properties for different ESR heats

ESR Heat No.		YS (0.2% PS) / MPa	UTS / MPa	Elongation / %	Reduction area / %	Impact strength at –40°C / J
Longitudinal requirement		1496 (Min.)	1793 (Min.)	10 (Min.)	30 (Min.)	25
Transverse requirement		1496 (Min.)	1793 (Min.)	5 (Min.)	25 (Min.)	25
E1	Long.	1482.4	1795.8	9.6	28.5	26, 24, 26
	Trans.	1467.3	1781.4	8.2	26.0	20, 24, 22
E2	Long.	1522.9	1832.6	10.8	33.6	28, 26, 27
	Trans.	1499.7	1805.8	9.5	30.0	25, 26, 26
E3	Long.	1531.8	1847.5	10.5	32.8	27, 26, 26
	Trans.	1506.0	1812.9	10.0	31.0	26, 25, 25
E4	Long.	1590.7	1946.7	11.4	39.4	42, 40, 42
	Trans.	1573.4	1905.8	11.8	36.4	38, 39, 38

Note: YS—yield strength; PS—plastic strain; UTS—ultimate tensile strength.

In this study, we used different processing routes to manufacture ESR heats E1, E2, E3, and E4. Hence, three different processing routes were used to manufacture AMS-4340 UHSS. Furthermore, for ESR heats E1, E2, and E3, a single antiflaking and homogenization cycle was used, whereas two homogenization and antiflaking cycles were used for ESR heat E4. Homogenization of ESR heat E1 was carried out for 14 h, where the homogenizations of ESR heats E2 and E3 were carried out for 12 h. We observed that the homogenization time for ESR heats E1, E2, and E3 was not sufficient to remove elemental segregation. Therefore, the homogenization time for ESR heat E4 was extended to 30 h before the start of forging. ESR heats E1, E2, and E3 were forged to the final required diameter in a single forging cycle, whereas two forging cycles were used for ESR heat E4. The two forging cycle routes followed in the case of E4 led to a better distribution of the alloying elements and to a decrease in elemental segregation. Further, ESR heats E1, E2, and E3 were subjected to a single AFT with a holding time of 5.3 h per inch of diameter. Hydrogen flakes were clearly observed in these heats. Moreover, ESR heat E4 was subjected to an additional AFT with a holding time of 9.5 h per inch. No hydrogen flakes and minimum elemental segregation (within acceptable limits) were observed for heat E4. Therefore, the processing route used to manufacture ESR heat E4 was the optimum processing path to develop AMS-4340 UHSS within the acceptable limits.

3.5. Cost estimation

In the present investigation, because of the non availability of a VIM + VAR process, an alternate route was explored. Thus, we compared the cost parameters of both processes. A cost review was performed for UHSS manufactured through VIM + VAR and air-melt + ESR routes. The cost of production through VIM was 1.5 times greater than that through conventional air melting. Next, during remelting in ESR and VAR, the operational cost of VAR was approximately 20% less than that of ESR because, unlike ESR, VAR does not use any prefused slag, which is costly. However, in the VAR process, both the electrode and VAR ingot require removal of surface impurities and nonmetallic inclusions by machining over their entire diameter, which results in 6%–8% loss in overall yield of the UHSS steel [6,24].

The electrode in ESR can be used in the as-cast condition, whereas the electrodes for VAR must be surface processed (e.g., ground or machined) for best cleanliness and to ensure that the surface layer contains few oxides. In both ESR and VAR, good chemical homogeneity and cleanliness were achieved. However, in VAR, the final ingot was 20% smaller than the starting ingot and electrode [25]. The energy consumption for the homogenization cycle of 25 tons of material to reach a soaking/homogenizing temperature of 1220°C was 69 SCM/ton (standard cubic meters/ton), whereas during soaking, the gas consumption was 17 SCM/ton. By contrast, for the AFT, the power consumption during heating to an antiflaking temperature of 680°C was 164 kW·h and that during soaking was 32 kW·h for 25 tons of material. Thus, the additional cost associated with a longer homogenization time and two AFT cycles is much lower than the cost associated with the VIM + VAR process.

4. Conclusions

Attempts to develop an alternate route for manufacturing AMS-4340 UHSS were successful. The main conclusions drawn from this study are as follows:

(1) The chemical composition of AMS-4340 was achieved in all of the ESR heats, although the least elemen-

tal segregation was observed for the ESR heat E4.

(2) Macrostructure evaluation revealed the presence of hydrogen flakes in ESR heats E1, E2, and E3, whereas no hydrogen flakes were observed in ESR heat E4. Microstructure characterization revealed that the hardening and tempering of the ESR heats refined their microstructure.

(3) Ultrasonic testing revealed no internal defects in ESR heat E4.

(4) ESR heat E4 achieved the best combination of mechanical properties. Thus, the processing route used for ESR heat E4 can be used as an alternate path to manufacture AMS-4340 UHSS without the use of a VIM + VAR process.

(5) The processing route suggested is more economical than the method currently used (VIM + VAR) for manufacturing UHSSs.

References

[1] S. Sharma, T. Nanda, M. Adhikary, T. Venugopalan, and B.R. Kumar, A simulation study of pearlite-to-austenite transformation kinetics in rapidly heated hot-rolled low carbon steel, *Mater. Des.*, 107(2016), p. 65.

[2] E.J. Pickering, Macrosegregation in steel ingots: The applicability of modelling and characterisation techniques, *ISIJ Int.*, 53(2013), No. 6, p. 935.

[3] Y. Liu, Z. Zhang, G.Q. Li, Q. Wang, L. Wang, and B.K. Li, The structural evolution and segregation in a dual alloy ingot processed by electroslag remelting, *Metals*, 6(2016), No. 12, p. 325.

[4] N.E. Prasad and R.J.H. Wanhill, *Aerospace Materials and Material Technologies*, Springer, Singapore, 2017, p. 401.

[5] A. Majumdar and S. Sadhukhan, Improvement in properties of Ni–Cr–Mo–V steel by process control, *Int. J. Mater. Metall. Eng.*, 10(2016), No. 6, p. 743.

[6] A. Choudhury, State of the art of superalloy production for aerospace and other application using VIM/VAR or VIM/ESR, *ISIJ Int.*, 32(1992), No. 5, p. 563.

[7] K. Steneholm, N.A.I. Andersson, A. Tilliander, and P.G. Jönsson, The role of process control on the steel cleanliness, *Ironmaking Steelmaking*, 45(2018), No. 2, p. 114.

[8] M. Ali, M. Eissa, H. El-Faramawy, D. Porter, J. Kömi, M.F. El-Shahat, and T. Mattar, Electroslag refining of CrNiMoWMnV ultrahigh-strength steel, *J. Miner. Mater. Charact. Eng.*, 5(2017), No. 6, p. 385.

[9] W.H. Johnson, On some remarkable changes produced in iron and steel by the action of hydrogen and acids, *Nature*, 11(1875), p. 393.

[10] J. Ćwiek, Prevention methods against hydrogen degradation of steel, *J. Achieve. Mater. Manuf. Eng.*, 43(2010), No. 1, p. 214.

[11] R.J. Fruehan, A review of hydrogen flaking and its prevention, *Iron Steelmaking*, 24(1997), No. 8, p. 61.

[12] K. Vrbek, J. Lamut, M. Marolt, and M. Knap, Changes in hydrogen content during steelmaking, *Arch. Metall. Mater.*, 60(2015), No. 1, p. 295.

[13] B.I. Voronenko, Hydrogen and flakes in steel, *Met. Sci. Heat Treat.*, 39(1997), No. 11, p. 462.

[14] L.A. Konopel'ko, A.M. Polyanskii, V.A. Polyanskii, and Y.A. Yakovlev, New metrological support for measurements of the concentration of hydrogen in solid samples, *Meas. Tech.*, 60(2018), No. 12, p. 1222.

[15] S. Dimitriu and C. Popescu, Causes for flakes appearance: preventing ways and removing methods, *Metalurgija.*, 9(2002), No. 1, p. 13.

[16] D.A. Mirzaev, N.I. Vorob'ev, O.K. Tokovi, D.V. Shaburov, and E.A. Fominykh, On the problem of hydrogen removal during heat treatment of large forgings, *Russ. Metall.*, 2006(2006), No. 1, p. 38.

[17] T.Z. Kattamis and M.C. Flemings, *Investigation of Solidification of High-strength Steel Castings* [Report], Department of Metallurgy, Massachusetts Institute of Technology, Cambridge, 1967.

[18] G.Y. Lai, W.E. Wood, R.A. Clark, V.F. Zackay, and E.R. Parker, The effect of austenitizing temperature on the microstructure and mechanical properties of as-quenched 4340 steel, *Metall. Trans.*, 5(1974), No. 7, p. 1663.

[19] C.R. Garr and A.R. Troiano, Flaking of heavy alloy steel sections, *JOM*, 9(1957), No. 4, p. 445.

[20] B. Arh, B. Podgornik, and J. Burja, Electroslag remelting: a process overview. *Mater Technol.*, 50(2016), No. 6, p. 971.

[21] G. Hoyle, *Electroslag processes: Principle and Practice*, Elsevier Science, 1983, p. 32.

[22] A. Sabih, P. Wanjara, and J. Nemes, Characterization of internal voids and cracks in cold heading of dual phase steel, *ISIJ Int.*, 45(2005), No. 8, p. 1179.

[23] R.C. Reed, *The Superalloys: Fundamentals and Applications*, Cambridge University Press, 2006, p. 122.

[24] R.L. Boxman, D.M. Sanders, and P.J. Martin, *Handbook of Vacuum Arc Science and Technology: Fundamentals and Applications*, Noyes Publications, 1995, p. 552.

[25] H. Scholz, U. Biebricher, H. Franz, A. Paderni, and P. Bettoni, State of the art in VAR and ESR processes — A comparison, [in] *International Conference Ingot Casting, Rolling and Forging*, Milan, 2014.